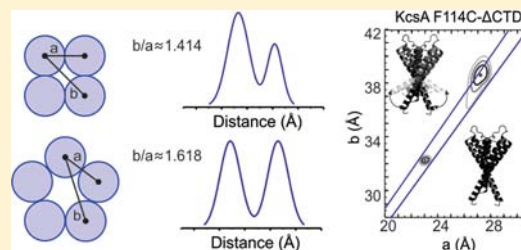


Symmetry-Constrained Analysis of Pulsed Double Electron–Electron Resonance (DEER) Spectroscopy Reveals the Dynamic Nature of the KcsA Activation Gate

Olivier Dalmas,[†] H. Clark Hyde,[†] Raymond E. Hulse, and Eduardo Perozo*

Department of Biochemistry and Molecular Biology, Institute for Biophysical Dynamics, The University of Chicago, 929 East 57th Street, Chicago, Illinois 60637, United States

ABSTRACT: Distance determination from an echo intensity modulation obtained by pulsed double electron–electron resonance (DEER) experiment is a mathematically ill-posed problem. Tikhonov regularization yields distance distributions that can be difficult to interpret, especially in a system with multiple discrete distance distributions. Here, we show that by using geometric fit constraints in symmetric homo-oligomeric protein systems, we were able to increase the accuracy of a model-based fit solution based on a sum of Rice distributions. Our approach was validated on two different ion channels of known oligomeric states, KcsA (tetramer) and CorA (pentamer). Statistical analysis of the resulting fits was integrated within our method to help the experimenter evaluate the significance of a symmetry-constrained vs standard model distribution fit and to examine multidistance confidence regions. This approach was used to quantitatively evaluate the role of the C-terminal domain (CTD) on the flexibility and conformation of the activation gate of the K⁺ channel KcsA. Our analysis reveals a significant increase in the dynamics of the inner bundle gate upon opening. Also, it explicitly demonstrates the degree to which the CTD restricts the motion of the lower gate at rest and during activation gating.



INTRODUCTION

Distance determination in macromolecules, and particularly in membrane proteins, is often at the core of arguments to decipher molecular mechanisms by which these nanomachines execute their biological function.^{1–3} In transporters, distance determination has been extensively used to decipher not only the extent of molecular motion but also the nature of the alternative access mechanism.^{4,5} The pulsed double electron–electron resonance (DEER) method is an unparalleled tool for measurement of long-range distances in proteins (20–80 Å).⁶ EPR offers several advantages over other spectroscopic techniques such as fluorescence resonance energy transfer (FRET). First, the small size of the spin label improves its accessibility to protein target sites. Second, the very short linker significantly improves probe localization by limiting the probe's diffusive region. Third, the same probe is used to label all target sites, which greatly simplifies the labeling strategy. Fourth, in DEER experiments, the signal is not polluted by possible under-labeling of the sample since the echo modulation arises exclusively from dipolar coupling. All these advantages translate into greater accuracy of probe position when applied to a macromolecule. The sensitivity and reliability of this technique depends on the optimization of the sample preparation, experimental conditions for measurement, and data analysis.^{4,5}

Analysis of DEER measurements yields a distance distribution obtained by either a model-free (e.g., Tikhonov regularization) or model-based fit. In this work, we improved model-based distance distribution analysis by utilizing the symmetry of homomeric proteins. Experimentally, all subunits

are spin-labeled at the same site. In such a multispin system, high precision distance determination has been obtained using a classical four pulse DEER protocol.⁷ However, broadening of the distance distribution may occur due to the signal contributions from the combinations of dipolar frequencies.⁸ Our geometric fit constraint method applies to a large class of proteins, including membrane proteins, which are often assembled into symmetrical multimeric entities. This is the case for Na⁺,⁹ Ca²⁺,¹⁰ K⁺,¹¹ Mg²⁺,¹² mechanosensitive,¹³ and ligand-gated ion channels.¹⁴ The inherent symmetry of subunit organization enables the fit of a model-based distance distribution function using the known organization of the protein in question.

Generating a distance distribution, $P(r)$, of interprobe distance r from a DEER signal is a moderately mathematically ill-posed problem, and as such, slight variations in the raw data's signal-to-noise ratio (SNR) can generate a large difference in the distance distributions.^{15,16} Tikhonov regularization is an elegant and widely used method for model-free analysis of DEER signal.¹⁷ Briefly, this technique minimizes the squared error between simulated and measured dipolar evolution by balancing smoothness and resolution of the distance distribution using a dampening term. Since the width of the distance distribution is not known in advance, the optimal regularization parameter λ must be selected (typically by the L-curve criterion¹⁸). Conversely, the distance distribution $P(r)$ can

Received: July 15, 2012

Published: September 4, 2012

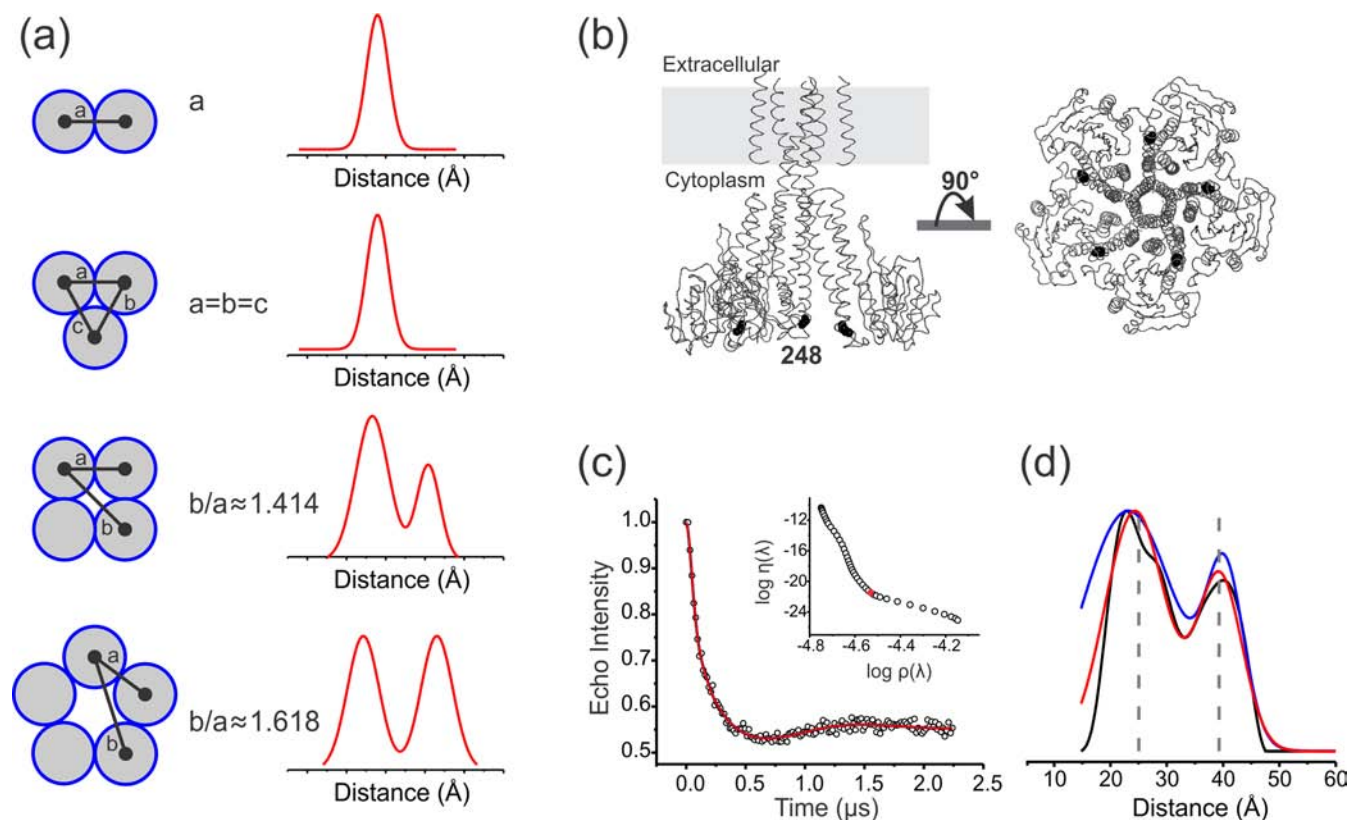


Figure 1. Distance determination in multimeric proteins. (a) Schematic representation of the expected distance distribution profile as a function of the oligomeric state of a homomeric protein. (b) Cysteine mutation in CorA is shown at position V248 as black spheres at C β . For clarity, only three subunits are shown. (c) The DEER refocused echo intensity is plotted (O) vs the evolution time. Fits determined from Tikhonov regularization, 2 Rice_{3D}, and symmetry-constrained 2 Rice_{3D} models are shown in black, blue, and red, respectively. In the inset, the optimal regularization parameter ($\lambda = 158$) is shown at the corner of the L-curve. (d) Corresponding distance distributions are plotted using the same color code. The vertical dashed lines represent the average spin–spin distances calculated from rotameric libraries of the spin label conjugated to the CorA V248C label site.³²

also be obtained by using a model-based approach, which has the advantage of enforcing smoothness and improving convergence, thereby improving the reliability of fitted distances provided that the chosen model is correct. Comparison and validation of any model-based fit to that of Tikhonov regularization is a critical component of such distance analysis. A recent study demonstrated that the interprobe distance distribution of two normally distributed spin labels is described by a three-dimensional Rice (Rice_{3D}) distribution rather than a Gaussian, which is especially important for accurate parameter estimation in broad distance distributions (e.g., $\mu/\sigma < 4$ with mean interprobe distance μ and standard deviation σ of each spin label position).¹⁹

In this study, we sought to incorporate the intrinsic symmetry of ion channels into model-based distance distribution fits. These homomeric proteins are each arranged as a regular convex polygon with m vertices (subunits). In the biologically relevant range of $m = 3$ – 6 , all geometries have vertex-to-vertex lengths characterized by one unique side (adjacent) and the following number of unique diagonals (d_m): $d_3 = 0$, $d_{4,5} = 1$, $d_6 = 2$. By symmetry, the number of expected peaks in the distance distribution $P(r)$ is equal to the sum of unique sides and diagonals ($1 + d_m$). Moreover, the diagonal and side lengths maintain a constant proportionality relation, independent of polygon size. In this paper, we consider the geometries for $m = 4$ and 5 , which both yield two unique mean distances between spin label paramagnetic centers, which we denote as $\langle r_1 \rangle$ for adjacent and $\langle r_2 \rangle$ for

diagonal. In these cases, there is only one proportionality constant, given by the mean distance ratio $\langle k \rangle = \langle r_2 \rangle / \langle r_1 \rangle$, and $P(r)$ is appropriately modeled by a two-component Rice_{3D} distribution. In the case of polygon models with $m > 6$, multiple distance ratios $\langle k_i \rangle$ exist. If we consider a homopentameric ($m = 5$) protein such as the Mg²⁺ channel CorA, where all subunits are spin-labeled at the same site, we expect $\langle k \rangle = (1 + \sqrt{5})/2 \approx 1.618$. Likewise, a homotetrameric ($m = 4$) assembly such as the K⁺ channel KcsA is expected to have $\langle k \rangle = \sqrt{2} \approx 1.414$. Expected distance distributions as a function of the oligomeric state are illustrated in Figure 1a. Given symmetric labeling, it is important to note that the mean distance ratio is equivalent for the mean position of the spin labels (e.g., nitroxide oxygen), as well as their corresponding labeling site (e.g., cysteine Ca).

We demonstrate that the distance ratio $\langle k \rangle$ can be utilized as a symmetry-based inequality constraint to (1) improve the model fit of a distance distribution $P(r)$ to DEER data and (2) aid interpretation of distances obtained from model-based fits. The method is especially suitable for poorly defined (flat) dipolar evolutions, as often obtained from flexible/dynamic systems. CorA V248C serves as an illustrative example of such a scenario (Figure 1b,c).

This new approach was implemented on two different ion channels of different oligomeric states, and the results are compared with other fitting methods (2 Rice_{3D} and Tikhonov regularization). We also performed a statistical analysis to compare the significance of different models and fitting procedures. The cross validation between our DEER data and

Table 1. Distance Determination Results for DEER Data Analyzed by Various Methods

cysteine mutant	distribution fit method	$\langle r_1 \rangle^{a,b}$	$\langle r_2 \rangle^{a,c}$	$\langle k \rangle$	fit rmsd	threshold rmsd ($\alpha = 0.05$)
CorA V248C	X-ray structure	26.0	41.3	1.588	<i>d</i>	
	Tikhonov ($\lambda = 158$)	22.8	40.35	1.770	0.0086750	
	2 Rice _{3D}	19.9 (± 9)	40.3 (± 3.3)	2.027	0.0086698	0.0090260
	2 Rice _{3D} [$1.578 \leq \langle k \rangle \leq 1.645$]	23.6 (± 4.9)	38.8 (± 4.2)	1.645	0.0088010	
CorA R252C	X-ray structure	24.2	38.0	1.570	<i>d</i>	
	Tikhonov ($\lambda = 31$)	24.2	39.1	1.616	0.0074304	
	2 Rice _{3D}	23.9 (± 2.2)	38.7 (± 1.8)	1.6185	0.0076829	0.0080159
	2 Rice _{3D} [$1.578 \leq \langle k \rangle \leq 1.645$]	23.9 (± 2.3)	38.7 (± 1.8)	1.6185	0.0076829	
KcsA R64C	2 Rice _{3D} [$1.367 \leq \langle k \rangle \leq 1.433$]	24.2 (± 1.4)	34.6 (± 5.5)	1.433	0.0125890	
	X-ray structure	22.0	32.0	1.454	<i>d</i>	
	Tikhonov ($\lambda = 10$)	22.0	31.8	1.445	0.0056134	
	2 Rice _{3D}	22.1 (± 0.7)	31.4 (± 3.6)	1.4212	0.0043960	0.0045779
	2 Rice _{3D} [$1.367 \leq \langle k \rangle \leq 1.433$]	22.1 (± 0.7)	31.3 (± 3.6)	1.418	0.0043963	
	2 Rice _{3D} [$1.578 \leq \langle k \rangle \leq 1.645$]	20.8 (± 3.3)	33.7 (± 2.7)	1.578	0.0061192	

^aValues reported in parentheses are fit values of σ_R from the 2 Rice_{3D} model (i.e., not distance confidence intervals). ^bAdjacent distance (Å). ^cDiagonal distance (Å). ^dNot applicable.

the corresponding X-ray structures provides a solid framework to study conformational changes associated with the gating mechanism of KcsA and CorA.

Taking advantage of our method we sought to monitor the influence of the C-terminal domain (CTD) helix bundle on the dynamics and the extent of motion of KcsA's activation gate. Upon proton-dependent activation, the K⁺ channel KcsA undergoes relatively large movements of its helical transmembrane segment TM2. These rearrangements have been extensively characterized by spectroscopic methods such as EPR,²⁰ fluorescence,²¹ solution NMR,²² and solid-state NMR,²³ and are in agreement with available open KcsA X-ray crystal structures.^{24,25} However, the influence of the CTD on the extent of the inner bundle gate opening has not been studied in the absence of either crystal lattice contacts or crystallographic chaperones. Here we found that in the absence of the CTD, the lower gate opening is significantly increased with respect to the full length channel, with a concomitant increase in protein dynamics upon activation. Our results are discussed in the context of the C-type inactivation mechanism and existing crystal structures.

MATERIALS AND METHODS

Protein Expression and Purification. Single cysteine mutants of *Thermotoga maritima* CorA (TmCorA) channels and *Streptomyces lividans* KcsA channels were expressed and purified as previously described.^{26,27} Briefly, after expression, the membrane fractions were solubilized with 10 mM DDM and loaded onto a pre-equilibrated cobalt affinity column (Clontech). During the purification, 5 mM β -mercaptoethanol and 0.5 mM TCEP were used to prevent cysteine oxidation. Immediately after protein elution with 250 mM imidazole, cysteine mutants were labeled with two additions of a 10-fold molar excess of MTSL spin label probes (Toronto Research Chemicals) on ice for 30 min sequentially. Labeled proteins were then further purified by size exclusion chromatography on a Sephadex G-200 column (GE Healthcare) previously equilibrated with buffer (Hepes 50 mM, pH = 7.0, NaCl 200 mM, MgCl₂ 40 mM, DDM 1 mM, for CorA mutants and Hepes 50 mM, pH = 7.0, or McIlVaine buffer (phosphate/citrate) pH = 3, KCl 200 mM, DDM 1 mM for KcsA mutants). The fractions containing the main monodisperse peak were collected and pooled together, supplemented with 20% glycerol, and concentrated to 100 μ M final concentration of oligomer assembly using a Millipore Centricon 30 kDa centrifugal filter unit.

DEER Experiment. Samples were loaded into a quartz capillary (Vitrocom) and equilibrated at 80 K under a flow of liquid N₂ using an

Oxford cryostat. A standard four-pulse DEER sequence was conducted on a Bruker Elexsys 580 EPR spectrometer equipped with a 3 mm split-ring resonator. The four-pulse DEER sequence was set with pulses of 16 ns (90°) and 32 ns (180°), and evolution times were typically set to 1800–2500 ns depending on distance and signal quality. The pump pulse was placed at the center peak of the spectrum, and the observation pulses were placed at a 75 MHz distance away on the low field side. Refocused echo intensity evolutions were recorded, and these phase-corrected signals were background-corrected assuming a homogeneous 3D distribution.

Distance Distribution Analysis. The distance distribution $P(r)$ was recovered from DEER measurements by three different approaches: model-free fit by Tikhonov regularization, model fit of a two-component Rice_{3D} mixture, or model fit of a two-component Rice_{3D} mixture with distance ratio constraint. For all approaches, the DeerAnalysis 2011 program¹⁶ was used for analysis with software modifications described below. Each time domain dipolar evolution data set was preprocessed using tools provided by DeerAnalysis to correct for experimental phase errors and to separate the intramolecular distances from the intermolecular background contribution. The background was subtracted from the dipolar evolution assuming a homogeneous distribution in three dimensions, appropriate for spin-labeled membrane proteins in detergent micelles. The origin of the background fit was determined by approximate Pake transformation in the frequency domain. The background-subtracted experimental dipolar evolution is referred to below as $V_{\text{exp}}(t)$.

Model-Free Distance Distributions by Tikhonov Regularization. For pulsed EPR measurements, Tikhonov regularization minimizes the following functional:⁶

$$G_{\lambda}(P) = \|K(r, t)P(r) - V_{\text{exp}}\|_2^2 + \left\| \lambda \frac{d^2}{dr^2} P(r) \right\|_2^2 \quad (1)$$

where $K(r, t)$ is a kernel that represents the ensemble average of the dipolar coupling over all possible molecular orientations for a given spin label radial separation r (and is the shape of a Pake double dipolar signal in the time domain); $P(r)$ represents the distance distribution of r . The first term on the right-hand side is the mean square deviation between the simulated and experimental dipolar evolution function; the second term on the right-hand side is the square norm of the second derivative of the distance distribution, which is multiplied by regularization parameter λ . Tikhonov regularizations were performed for a logarithmic sequence of regularization parameters on the range $\lambda = [10^{-3}, 10^3]$ with 4 points per decade. The optimal regularization parameter λ was calculated from this set of solutions by applying the L-curve criterion of maximum curvature.¹⁸ For all data sets, the optimal λ was confirmed to be located at the corner of the L-curve by visual inspection. Parameters from Tikhonov regularization solution at

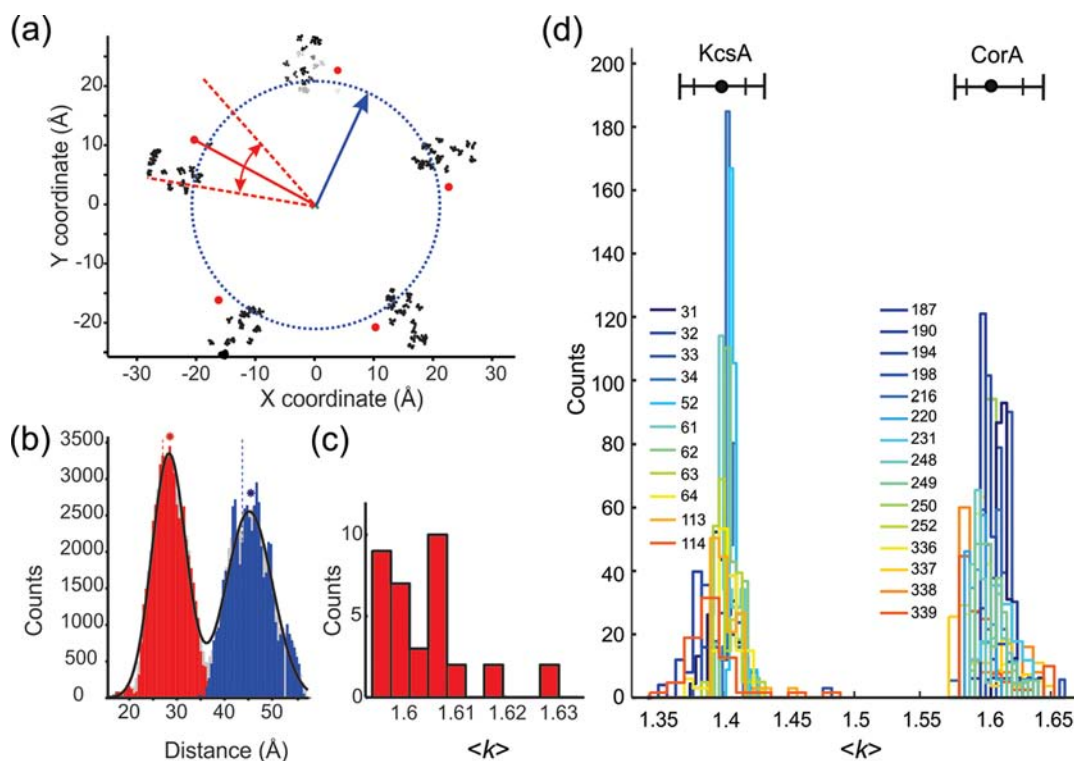


Figure 2. Rotamer-based simulation of distance ratio distribution for KcsA and CorA. (a) MTSL rotamers were attached to CorA at position 252 using the program MMM.³² Nitroxide oxygen coordinates were oversampled (see text) and are displayed as black dots. CorA 252C *Ca* are represented as red dots, and the channel's symmetry axis is marked at the origin as a green cross. MTSL rotamer clouds were independently modified by exclusion of points based on a linear scan of occupancy (step = 0.01), radial distance (step = 0.5 Å), and cylindrical angle (step = $\pm 0.3^\circ$). For visualization of occupancy, rotamers in the uppermost subunit were grayscale (black = high; white = low). The blue circle (dotted) and arrow represent the radial distance scan. The red lines (dashed) and arrows represent the cylindrical angle scan. (b) Distance histograms are shown to exemplify one MTSL cloud modification for one mutant; r_1 is red, r_2 is blue, and their combination is gray. Asterisks represent the mean of the distribution using the same color code; vertical dotted lines represent *Ca* distances. A 2 Rice_{3D} fit of the combined distribution is displayed in black. (c) Histogram of $\langle k \rangle$ from the set of all MTSL cloud modifications for one mutant. (d) Histograms of $\langle k \rangle$ from the set of all MTSL cloud modifications for 11 KcsA (tetramer) and 15 CorA (pentamer) mutants. For both channels, the average $\langle k \rangle$ is plotted as a black circle, and 1–99% and 5–95% intervals are plotted as tall and short ticks, respectively.

optimal λ were analyzed and reported in Table 1. All data set solutions had a distribution $P(r)$ comprised of two primary distance peaks. The first peak (shorter distance) was interpreted as the mean adjacent distance r_1 and the second peak (longer distance) was interpreted as the mean diagonal distance r_2 .

Model-Based Distance Distributions by Three-Dimensional Rice Mixture. A model fit minimizes the following functional:

$$G(P) = \left\| K(r, t) P_{\text{model}}(r; \theta) - V_{\text{exp}} \right\|_2^2 \quad (2)$$

where θ is a parameter vector that defines the probability density function of an analytical model distribution. Here, dampening is inherently introduced by the smooth distance distribution, $P_{\text{model}}(r; \theta)$. The interprobe distance $r = (\Delta x^2 + \Delta y^2 + \Delta z^2)^{1/2}$ between two spin label centers, each normally distributed in space (x, y, z) with standard deviation σ_S about its center, is described by the Rice_{3D} distribution,^{28,29} generalized to n -dimensions as

$$f_n(r; \mu, \sigma_R) = \frac{r^{(n/2)}}{\mu^{(n/2)-1} \sigma_R^2} \exp\left[\frac{-(r^2 + \mu^2)}{2\sigma_R^2}\right] I_{(n/2)-1}\left(\frac{r\mu}{\sigma_R^2}\right), \quad r \geq 0 \quad (3)$$

where the mean interprobe distance $\mu > 0$ and Rice standard deviation $\sigma_R > 0$ are real numbers; n is the dimension of the spin label normal random variables ($n = 3$ for labeled membrane proteins in detergent micelles); I_v denotes the modified Bessel function of the first kind of real order v . Assuming all spin labels have equal spatial variance, the Rice standard deviation is related to the spin label spatial standard

deviation by $\sigma_R = 2^{1/2} \sigma_S$, which is a correction from that reported in ref 30. The Rice_{3D} distribution can be simplified³⁰ to a more computationally efficient form using the relation $I_{1/2}(x) = [2/(\pi x)]^{1/2} \sinh(x)$:

$$f_3(r; \mu, \sigma_R) = \frac{r}{\mu \sigma_R} \sqrt{\frac{2}{\pi}} \exp\left[\frac{-(r^2 + \mu^2)}{2\sigma_R^2}\right] \sinh\left(\frac{r\mu}{\sigma_R^2}\right), \quad r \geq 0 \quad (4)$$

The probability density function of the two-component mixture of Rice_{3D} distributions is

$$P(r; \theta) = w f_3(r; \mu_1, \sigma_{R,1}) + (1 - w) f_3(r; \mu_2, \sigma_{R,2}), \quad r \geq 0 \quad (5)$$

where w is the fraction of the first mixture component and $\theta = (\mu_1, \sigma_{R,1}, \mu_2, \sigma_{R,2}, w)$ is the set of all parameters that defines the bimodal distance distribution. The probability density function $P(r; \theta)$ was fit to $V_{\text{exp}}(t)$ by minimization of eq 2 using nonlinear least-squares regression.

Symmetry-Constrained Model Fit and Software Modification. DeerAnalysis 2011 software¹⁶ was modified and supplemented in MATLAB (The MathWorks, Inc.) to introduce the use of nonlinear inequality constraints into the nonlinear minimization problem of fitting a model-based distance distribution to a measured dipolar evolution data set using eq 2. We primarily added the ability to perform constrained two-component Rice_{3D} and two-component Gaussian mixture model fits where the mean distance ratio $\langle k \rangle = \langle r_2 \rangle / \langle r_1 \rangle = \mu_2 / \mu_1$ is constrained within user-defined limits $[k_{\text{min}}, k_{\text{max}}]$

relevant to known symmetry of the protein under investigation. For model fits of a distance distribution, DeerAnalysis 2011 performs minimization in the least-squares sense using the built-in MATLAB function *fminsearch* with simplex search method. We implemented model fitting with nonlinear inequality constraints using the built-in MATLAB function *fmincon* with active-set algorithm. Both functions were verified to return the same solution when used under equivalent conditions. The ability to perform model fits with nonlinear inequality constraints will be implemented in a future release of DeerAnalysis software,¹⁶ available from ETH Zurich, <http://www.epr.ethz.ch/software/>.

RESULTS AND DISCUSSION

A Symmetry-Derived Nonlinear Constraint To Fit DEER Measurements. A poorly defined (flat) dipolar evolution is difficult to transform into a reliable distance distribution (Figure 1c). Here, we sought to incorporate intrinsic symmetry of homomeric ion channels into model-based distance distribution fits. Both homotetrameric and homopentameric assemblies have an adjacent $\langle r_1 \rangle$ and diagonal $\langle r_2 \rangle$ distances related by the ratio $\langle k \rangle = \langle r_2 \rangle / \langle r_1 \rangle$ with theoretical values of 1.414 and 1.618, respectively (Figure 1a). Of course in nature, symmetry is never perfect, and membrane proteins are no exception. Simple measurement of C β –C β distances from the CorA crystal structure³¹ illustrates this deviation, resulting in a k interval of 1.57–1.68. In addition, spin labels could adopt different rotameric configurations, which could distort the symmetry of the labels within a single protein. Combined with thermal motion, these observations support the idea that the distance ratio must be contained within two limits, rather than at a fixed value. Accordingly, we sought to evaluate in a rational and quantitative manner the distribution of $\langle k \rangle$. Accordingly, we selected a total of 26 positions distributed along the sequence of KcsA and CorA and used an *in silico* spin-labeling technique via the software MMM.³² For each mutant tested, the selected residue was mutated to cysteine and MTSL was attached with the 26 most probable rotameric conformations, thus producing a cloud of possible spin label conformations on each channel subunit. The nitroxide oxygen (O1) atom was used as a proxy to the position of the paramagnetic center of the probe. To slightly smooth the MTSL O1 distance distribution and account for minimal conformational relaxation, each O1 point was replicated 5 times with a small amount of random noise added (sample points were randomly drawn from a uniformly distributed sphere with 0.5 Å radius, centered at the actual O1 position). To evaluate the effect on $\langle k \rangle$ from MTSL cloud distortion caused by conformational change or spin label rotameric freedom, we implemented simulation tools to sequentially include or exclude rotameric conformations based on three criteria: (1) occupancy, (2) O1 radial distance to the symmetry axis, and (3) O1 cylindrical angle with respect to the labeled cysteine C α (Figure 2a). The influence of these three parameters was homogeneously assayed by our sampling conditions such that only uniquely modified MTSL clouds were analyzed. For each modification condition, we calculated $\langle k \rangle$ and a histogram of all unique intersubunit O1–O1 distances that could be successfully fit by a 2 Rice_{3D} model distribution (Figure 2b). From the set of all MTSL cloud modification conditions, we obtained a histogram for $\langle k \rangle$ (Figure 2c). The final result of this simulation analysis performed on all KcsA and CorA mutants is presented in Figure 2d. Remarkably, we found that the distance ratio remained extremely close to theoretical values: $\langle k \rangle = 1.402$ for KcsA and $\langle k \rangle = 1.605$ for CorA. Moreover, despite our efforts

to distort the rotameric spatial distribution of spin labels at their binding site, the distribution of $\langle k \rangle$ remained tight. The 1–99% $\langle k \rangle$ interval for all mutants tested was 1.367–1.433 for KcsA and 1.578–1.645 for CorA (Figure 2d). We assumed that the extensive number of labeling sites tested in addition to the comprehensive sampling strategy leads to a robust and reliable $\langle k \rangle$ distribution. Henceforth, we refer to this exercise as rotamer simulation.

Symmetry-Constrained Analysis of a Broad Distance Distribution. We sought to compare the experimentally derived $P(r)$ from a poorly defined dipolar evolution obtained from CorA V248C analyzed by three different fit methods: Tikhonov regularization, 2 Rice_{3D}, and symmetry-constrained 2 Rice_{3D} (see Materials and Methods). Figure 1c shows that fits of the background-subtracted dipolar evolution by these three methods are almost indistinguishable visually, and have fairly similar root-mean-square deviation (rmsd) values (Table 1). However, the corresponding set of distance distributions are substantially different (Figure 1d). When we imposed rotamer simulation-based limits on the distance ratio ($\langle k \rangle = 1.578$ –1.645) to stabilize the correct solution, we obtained adjacent and diagonal distances that both agree remarkably well with the distances calculated from the CorA crystal structure¹² using a rotameric library of the spin label.³² Notice that $P(r)$ obtained by Tikhonov regularization is distorted from the idealized distribution, illustrated by emergence of a third peak. We argue that this deviation from an idealized distance distribution is purely artificial and is not a true reflection of the structural dynamics of the system. This reasoning is based on the observation that when the dipolar evolution is better defined, that is, when more periods are detected, $P(r)$ calculated from a Tikhonov fit is virtually equivalent to a 2 Rice_{3D} distribution (see Figure 3). Recently, an improved dipolar evolution was

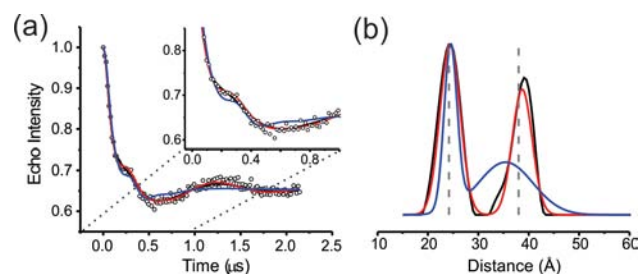


Figure 3. Validation of the symmetry-constrained model fit method. (a) The background-subtracted dipolar evolution (O) obtained for the CorA R252C mutant was fit using three different methods: Tikhonov regularization ($\lambda = 31$) is shown in black, a 2 Rice_{3D} fit with distance ratio $\langle k \rangle = 1.578$ –1.645 is shown in red, and a 2 Rice_{3D} fit intentionally misconstrained such that $\langle k \rangle = 1.367$ –1.433 is shown in blue. The inset is a magnification to better illustrate fit disparities. (b) The corresponding distance distributions are shown using the same color code. The dashed vertical lines correspond to average distances calculated from the X-ray structure.³¹

demonstrated by a groundbreaking paper by the Hubbell group where they used a bifunctional probe, which reflects the motion of the protein with greater accuracy. When they compared $P(r)$ obtained with the bifunctional vs classical probe at an equivalent position, they obtained a sharper distribution and homogeneous peak shape.³³ This result supports the idea that our approach of using a symmetry-constrained 2 Rice_{3D} model to derive the distance distribution is an idealization rather than an oversmoothing of the data. It is important to note that all

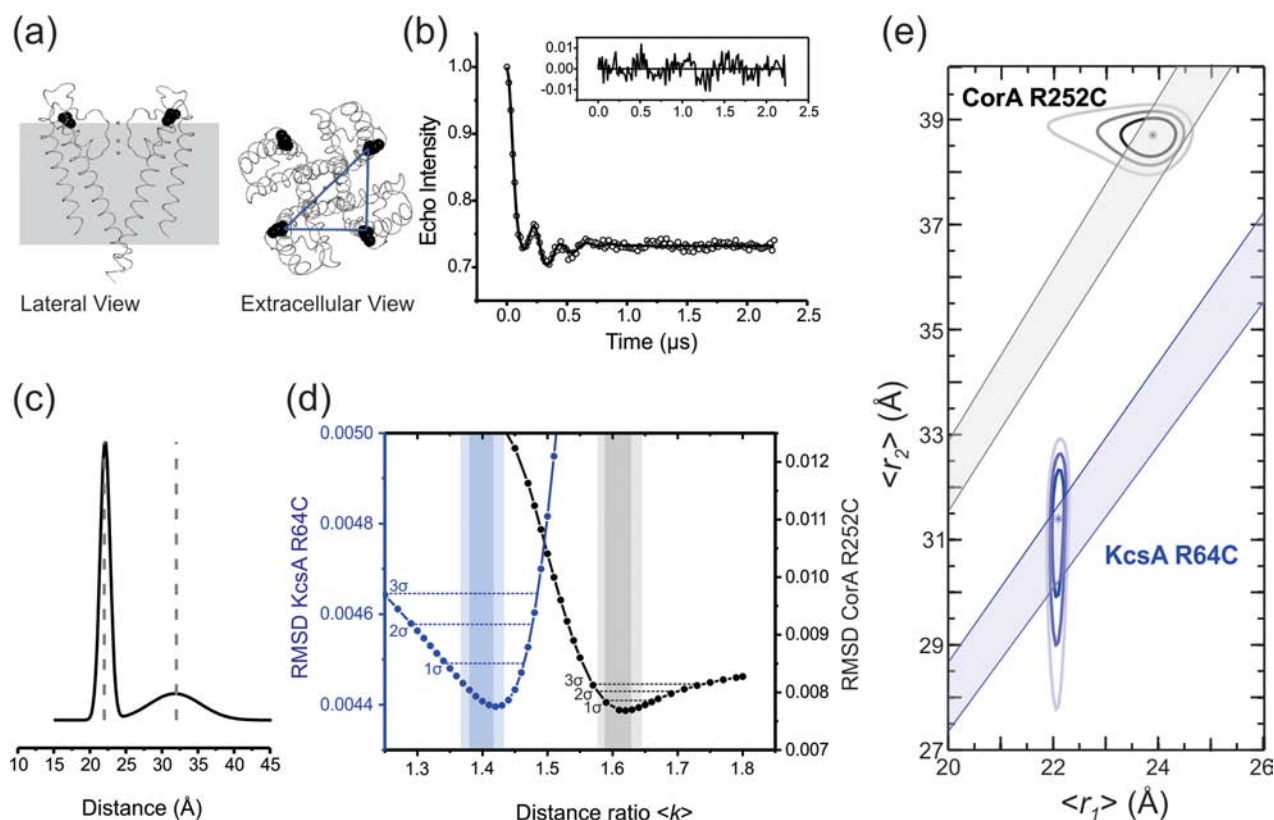


Figure 4. DEER measurements from the homotetrameric K^+ channel KcsA R64C and distance confidence regions. (a) The R64 residue is shown in black on a ribbon representation of the X-ray structure.⁴⁰ (b) The background-corrected dipolar evolution is shown as open circles and the fitted dipolar evolution from a 2 Rice_{3D} model is plotted as a solid line; fit residuals are shown in the inset. (c) The corresponding distance distribution is shown as a solid line together with the expected distances (dashed lines) from the crystal structure. (d) The error surface of the distance ratio $\langle k \rangle$ from 2 Rice_{3D} model fits of KcsA R64C (blue) and CorA R252C (black). Distance ratio confidence intervals by F-test at $\alpha = 0.32$ (1σ), $\alpha = 0.05$ (2σ), and $\alpha = 0.003$ (3σ) significance levels are shown as dashed horizontal lines. Shaded areas represent the 5–95% and 1–99% $\langle k \rangle$ intervals determined by rotamer simulation. (e) Plots of the 68%, 95%, and 99.7% approximate confidence regions of mean distances $\langle r_1 \rangle$, $\langle r_2 \rangle$ obtained by 2 Rice_{3D} model analysis of DEER measurement from CorA R252C and KcsA R64C. The asterisk is positioned at the optimal parameter set $\hat{\theta}$. Shaded areas represent the 1–99% $\langle k \rangle$ intervals.

mathematical tools used to extract $P(r)$ require a certain smoothness of the distribution.⁶ Several algorithms have shown that the introduction of constraints and smoothing in the distance domain can stabilize the solution. This has been shown for the approximate Pake transformation³⁴ and is also at the core of Tikhonov regularization.^{16,35}

Statistical Analysis of Symmetry-Constrained Distance Distributions. Since oversmoothing the fit of the data is a legitimate concern, we sought to investigate the influence of our symmetry-constrained model on a more well-defined CorA mutant data set. Here, we chose the CorA cysteine mutant R252C that yields data of much better quality compared with V248C, that is, a well-defined background-corrected dipolar evolution (Figure 3a). In this case, we observed no substantial difference between $P(r)$ generated by Tikhonov regularization or by the 2 Rice_{3D} model approach (Figure 3b). Interpretation of distances obtained by a symmetry-constrained model fit requires statistical analysis of the goodness of fit. A generalized model distribution function can be defined by parameter vector $\theta = (\theta_1, \theta_2, \dots, \theta_p)$ with p fitted parameters. In the absence of a symmetry constraint, the least-squares estimate of θ , denoted by $\hat{\theta}$, minimizes the error sum of squares (S) between the experimental and simulated dipolar evolution. Note that application of a symmetry constraint does not alter the number of free parameters. In

this case, the statistical significance of a constrained nonlinear regression can be assessed by the likelihood-ratio criterion, which defines the $100(1 - \alpha)\%$ confidence region^{36,37} of the parameters as

$$S(\theta) = S(\hat{\theta}) \left(1 + \frac{p}{n-p} F_{p, n-p}^\alpha \right) \quad (6)$$

where the dipolar evolution has n observations and $F_{p, n-p}^\alpha$ is the upper critical value of the $F_{p, n-p}$ distribution at significance level α . Equation 6 defines a threshold at which variation of the parameters causes a fractional increase in S that is statistically significant at level α , typically set at $\alpha = 0.05$ (2σ), and assumes that observations are independent.

The likelihood ratio allows rigorous estimation of parameter uncertainty by error surface analysis.³⁸ The procedure is to first obtain the optimal parameter set $\hat{\theta}$ from a standard (unconstrained) model fit with minimum error, that is, $S(\hat{\theta})$ or $\text{rmsd}(\hat{\theta})$. Next, the selected parameter is incremented away from its optimal value by a fixed step size, and the regression is repeated (with all other parameters simultaneously optimized). This process continues until the fit error exceeds the threshold value. The parameter value that defines the exact confidence interval boundary is obtained by quadratic interpolation. This procedure is then repeated in the opposite direction to obtain the opposite boundary.

By inversion, the likelihood ratio also gives an F-test to determine whether the model fit is significantly different in constrained vs standard form. This F-test thus has the null hypothesis $H_0: \theta = \hat{\theta}$ and alternative hypothesis $H_A: \theta \neq \hat{\theta}$. For example, if a symmetry-constrained fit yields $S(\theta)$ that is greater than the right-hand side of eq 6, the parameter set is significantly different. We analyzed our data using the DeerAnalysis program,¹⁶ which reports goodness of fit by rmsd. Therefore we used the equivalent form of eq 6 to calculate all F-test threshold values reported in Table 1:

$$\text{rmsd}(\theta) = \text{rmsd}(\hat{\theta}) \sqrt{1 + \frac{p}{n-p} F_{p, n-p}^{\alpha}} \quad (7)$$

This F-test allows us to compare, without bias, the goodness of fit between a symmetry-constrained and standard form of the same model. As a proof of principle of this F-test, we intentionally misconstrained our fit of the R252C data set using a 2 Rice_{3D} distribution with distance ratio $\langle k \rangle = 1.367\text{--}1.433$ (from rotamer simulation), as if CorA was a tetramer (Figure 3). As anticipated, the small variation in the fit of the dipolar evolution translates into a dramatic change in the distance distribution. The values reported in Table 1 show that the incorrect model has rmsd above the F-test threshold, letting the user know that the model fit is significantly different (worse) at $\alpha = 0.05$. This demonstrates that the use of this F-test gives the user a valid and useful approach to compare different models and fitting procedures for analysis of DEER data.

Validation on a Homotetrameric K⁺ Channel. We further validated the method on another membrane protein harboring a different oligomeric state. We chose the well characterized K⁺ channel KcsA because we can easily compare the DEER-derived distance distribution against its well-accepted crystal structure.³⁹ The residue R64, located in the outer vestibule of KcsA, has already been shown to be suitable for DEER measurement and was therefore our first choice.⁷ Remarkably, as illustrated in Figure 4, we were able to find excellent agreement between our R64C data set fit by a 2 Rice_{3D} distribution constrained by $\langle k \rangle = 1.367\text{--}1.433$, the crystal structure,⁴⁰ and previously reported DEER measurements⁷ (Table 1). As another proof of principle for the F-test, we observed that when we intentionally misconstrained the fit with distance ratio $\langle k \rangle = 1.578\text{--}1.645$, as if KcsA was a pentamer, the rmsd exceeds the F-test threshold value at $\alpha = 0.05$. Interestingly, the distance ratio error surface (rmsd vs $\langle k \rangle$) shows that the error minimum is located close to the theoretical $\langle k \rangle$ value for both systems (CorA and KcsA). There are several important observations that apply to both systems: (1) the theoretical $\langle k \rangle$ values are contained within their respective 95% confidence intervals, and (2) there is no overlap between 95% confidence intervals of $\langle k \rangle$ (Figure 4d). This result indicates that the $\langle k \rangle$ from a 2 Rice_{3D} fit can be used to distinguish between a homotetrameric and a homopentameric assembly. It also suggests that a 95% confidence interval (2σ) is likely to be the best compromise between statistical significance and stringency.

Distance Confidence Regions as a Measure of Uncertainty for DEER Measurements. The ability to perform an F-test on the rmsd from a DEER fit allowed us to determine distance confidence regions for model-based fits of our DEER data. Distance confidence region analysis conveys the most complete representation of the confidence of recovered distances. Figure 4e shows various confidence

regions for mean distances ($\langle r_1 \rangle$, $\langle r_2 \rangle$) obtained by 2 Rice_{3D} analysis of CorA R252C and KcsA R64C data sets. Each data set was fit by the model at fixed combinations of mean distance ($\langle r_1 \rangle$, $\langle r_2 \rangle$) within a uniformly spaced 2D grid of test points that encompassed the solution basin. At each test point ($\langle r_1 \rangle$, $\langle r_2 \rangle$), all other parameters were simultaneously optimized. The rmsd from the set of grid solutions was then interpolated (cubic) at 10× higher resolution to obtain a smooth expectation surface, followed by isocontour evaluation at selected levels of significance. The 100(1 - α)% confidence interval of a selected parameter (e.g., $\langle r_1 \rangle$), can be obtained by projection of the 100(1 - α)% confidence region onto the selected parameter axis. For these well-defined data sets, several observations can be made about the Rice_{3D} model and its parameter estimation. First, the optimal solution (and the majority of the 68% confidence region) lies within the respective $\langle k \rangle$ intervals obtained by rotamer simulation. Second, the confidence regions are approximately elliptical, with slight distortion for the CorA R252C data set, indicating low degree of nonlinearity (a linear model has elliptical confidence regions). Third, the relative roundness of the confidence regions indicates stable parameters, which means that the estimation precision of both distance parameters is balanced, and there is low parameter-effect curvature (i.e., well-conditioned parametrization). Fourth, the small off-axis tilt of the confidence regions indicates low parameter correlation. Combined, these observations validate our proposed use of statistical inference for the 2 Rice_{3D} model.

Influence of the C-Terminal Domain on Activation Gating of KcsA. The activity of ion channels is often regulated by interaction with ligand or other subunits via their cytoplasmic domain (N- or C-terminus). For example, Ca²⁺ activation of BK channels is mediated through its binding at the cytoplasmic domain RCK.^{41,42} In some prokaryotic K⁺ channels, the cytoplasmic domain plays an important role in protein folding and thermal stability.^{43–45} The KcsA CTD directly connects to the gating transmembrane helices TM2 and folds as a four-helix bundle that projects ~70 Å into the cytoplasm.^{45,46} Using a chaperone-assisted crystallography approach, the structure of the full-length (FL) KcsA was recently solved in an open/inactivated conformation.²⁵ These studies have revealed that the CTD remains a four-helix bundle during the gating process and by exerting a physical strain on the lower gate restricts the motion of the gating helices.^{24,25} This observation correlates well with the increased rate and extent of C-type inactivation when the CTD is truncated.⁴⁷ Moreover, binding of crystallographic chaperones (Fab fragments) has functional consequences, slowing down the rate of C-type inactivation.²⁵ Since C-type inactivation is mechanically coupled to the opening of the lower gate,^{24,47} it is reasonable to propose that the Fab fragment used for crystallography provides additional strain on the lower gate that would further stabilize the closed conformation.

Taking advantage of our ability to reliably determine distance in homomeric proteins, we sought to monitor the influence of the KcsA CTD on the extent of lower gate opening in the absence of any antibody or artificial crystal lattice contact. The outward facing position 114 located at the lower gate was an ideal reporter candidate because interprobe separation is compatible with the distance range of the DEER technique (20–80 Å). The experiments were conducted for both constructs (FL and Δ CTD) at pH = 7, which stabilizes the closed state, and at pH = 3, which favors the open conformation. In the closed state (pH = 7), the truncation of

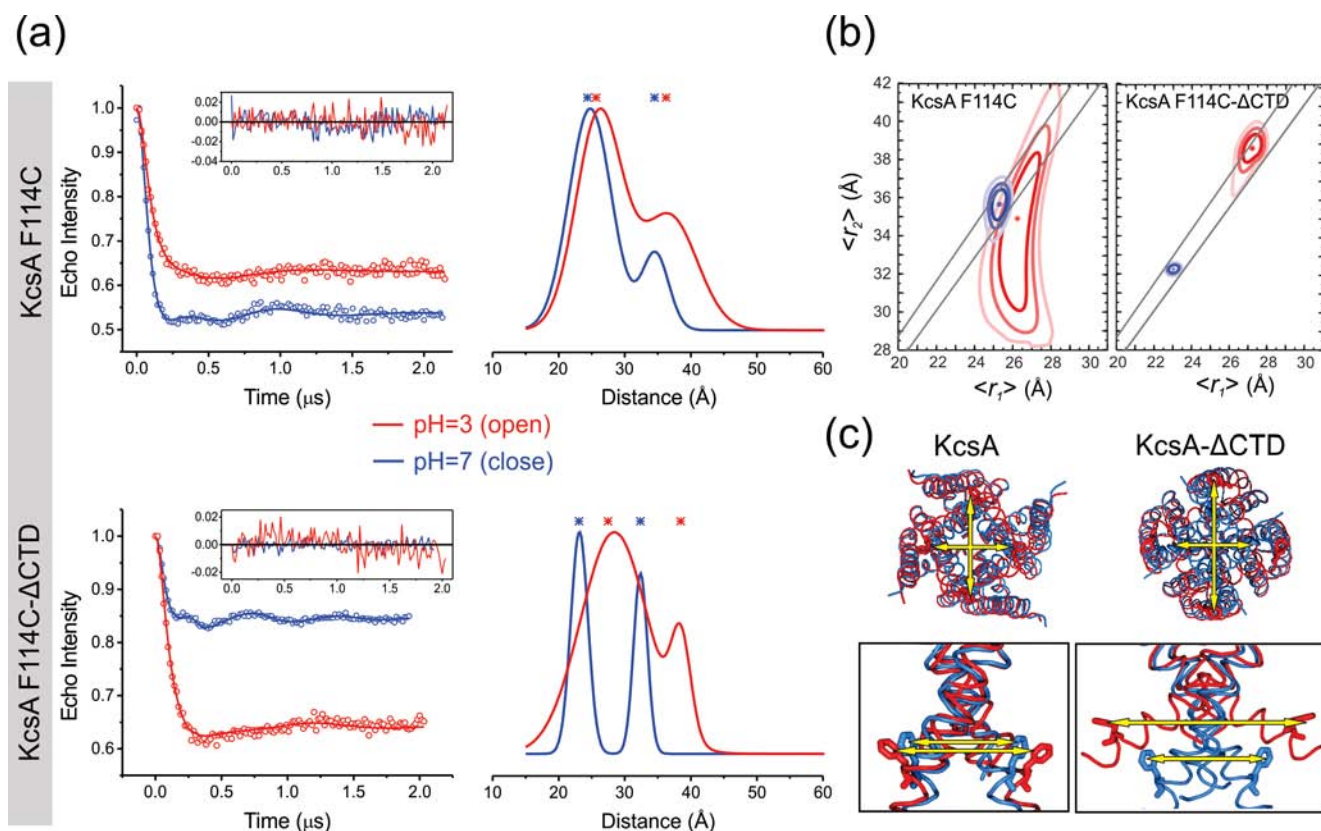


Figure 5. Influence of the C-terminal domain on activation gating of KcsA. (a) Background-subtracted dipolar evolution of KcsA-F114C FL and Δ CTD are shown in upper and lower panels, respectively. Data recorded at pH = 3 and pH = 7 are shown in red and blue, respectively. For each construct, the inset displays the fit residuals and the right panel shows the corresponding distance distribution obtained by a symmetry-constrained 2 Rice_{3D} model fit constrained with $\langle k \rangle = 1.367\text{--}1.433$. For each data set, $\langle r_1 \rangle$ and $\langle r_2 \rangle$ are shown by asterisks. (b) Plots of the 68%, 95%, and 99.7% approximate confidence regions of mean distances ($\langle r_1 \rangle$, $\langle r_2 \rangle$), obtained by symmetry-constrained 2 Rice_{3D} model analysis of DEER measurements from KcsA-F114C FL and Δ CTD. Measurements obtained at pH = 7 (closed) and pH = 3 (open) are colored blue and red, respectively. An asterisk is positioned at each optimal parameter set $\hat{\theta}$. The two diagonal lines represent the 1–99% (k) interval (1.367–1.433). (c) KcsA closed (3EFF)⁴⁶ and open (3PJS)²⁵ structures are aligned and ribbon-represented using the same color code view from the cytoplasmic side. The inset shows a magnified lateral view of the activation gate where F114 is stick-represented. An analogous representation for the truncated channel is shown in the lower panels using 1K4C³⁹ and 3F7V²⁴ PDB accession codes.

Table 2. Distance Determination at KcsA Activation Gate from Constrained 2 Rice_{3D} Analysis

construct	experimental conditions	$\langle r_1 \rangle^{a,b}$	$\langle r_2 \rangle^{a,c}$	fit rmsd	threshold rmsd ($\alpha = 0.05$)
KcsA F114C	pH = 7 (closed)	25.3 (± 3)	35.6 (± 1.8)	0.0088333	0.0092203
	pH = 3 (open)	26.5 (± 2.9)	36.2 (± 4.5)	0.0087260	0.0090727
KcsA F114C- Δ CTD	pH = 7 (closed)	23.1 (± 1.3)	32.3 (± 1)	0.0029793	0.0031230
	pH = 3 (open)	27.5 (± 5.3)	38.6 (± 1.2)	0.0062729	0.0065581

^aValues reported in parentheses are fit values of σ_R from the 2 Rice_{3D} model (i.e., not distance confidence intervals). ^bAdjacent distance (\AA). ^cDiagonal distance (\AA).

the CTD is known to produce a substantial structural rearrangement of the lower gate as detected semiquantitatively by FRET⁴⁷ and revealed in further detail by X-ray crystallography.⁴⁶ Our DEER experiments for F114C clearly show that the interprobe distances change at pH = 7 when KcsA is truncated (Figure 5 and Table 2). The mean distances ($\langle r_1 \rangle$, $\langle r_2 \rangle$) decrease from (25.3, 32.3 \AA) for the FL channel to (23.1, 35.6 \AA) for the Δ CTD channel. Although small, this modest rearrangement is reliably reported by our DEER experiment because there is no overlap of the distance confidence regions at the 99.7% (3σ) confidence level (Figure 5b). This distance difference seems fully compatible with the 15° outward tilting of TM2 after residue 110 observed by

crystallography when truncated structures are compared with the full length channel.⁴⁶

In the full length channel, we observe a very modest change in interprobe distances when the channel is triggered to open (Figure 5a). In the open state, the dipolar evolution is flatter and the distance ratio constraint $\langle k \rangle$ is necessary to find a satisfactory solution (Figure 5). The confidence region analysis revealed no overlap at the 68% (1σ) level in the allowed distance region between the pH = 7 and pH = 3 data sets. However, there is a significant overlap at the 95% (2σ) level, indicating that uncertainties of the DEER measurements at this confidence level are greater than the inferred motion when KcsA-FL opens.

One major conclusion of the experiment is that the CTD truncation allows wider opening of the activation gate at position 114. This is evidenced by the large change in the distance distribution of TM2. During opening, the mean interprobe distance change is more than 6 Å for the diagonal distance: $(\langle r_1 \rangle, \langle r_2 \rangle)$ increases from (23.1, 32.3 Å) at pH = 7 to (27.5, 38.6 Å) at pH = 3 (Figure 5 and Table 2). Several KcsA- Δ CTD open structures have been crystallized, with lower gate openings (using T112 C α -C α diagonal distance as a reporter) ranging from 15 to 17, 23, and 32 Å open (the closed state being 12 Å).²⁴ The activation mechanism is largely compatible with CW-EPR²⁰ and solid-state NMR^{23,48} conducted in the presence of a lipid bilayer, reinforcing the idea that crystallography has captured relevant conformations. The average distance change observed by DEER seems in excellent agreement with the intermediate opening states (structures 15 and 17 Å open) captured by crystallography²⁴ with the mean diagonal distance changes in C α -C α at residue T112 to be ~6–8 Å from the closed state.

Interestingly, the dipolar evolution from F114C obtained in the open state (pH = 3) is systematically flatter than its closed state (pH = 7) counterpart, leading to a much broader distance distribution. This observation is consistent with an increase in protein dynamics represented by wider swings of the inner bundle helices. The broad range of opening captured by crystallography is likely correlated to the wider distance distribution observed by DEER spectroscopy at pH = 3. This suggests that upon activation, the lower gate is sampling a larger conformational space than when the channel is closed. This observation is not likely to arise from an increase in probe dynamics, because the probe mobility does not increase noticeably upon activation as measured by CW-EPR.²⁰ Since the opening of the inner bundle helices is physically coupled to the inactivation of the selectivity filter via allosteric coupling,⁴⁷ determining the correlation between the dynamics of the lower gate and the conformational fluctuations of the selectivity filter represents an important step toward the detailed understanding of ion conduction and C-type inactivation in K⁺ channels.

CONCLUSIONS

In summary, we have implemented a simple but efficient strategy to stabilize the fitting solution of DEER data using the implicit organization of homomeric proteins. The methods described here will be available in a future release of DeerAnalysis software,¹⁶ available at <http://www.epr.ethz.ch/software/>. The symmetry-constrained model fit allows quantitative and statistical evaluation of theoretical vs experimentally derived distance distributions. We have experimentally shown that our approach is valid for a homotetramer as well as for a homopentamer. We hope that the method presented here will be particularly advantageous for challenging targets and highly dynamic systems where the distance distributions are broader and thus more difficult to accurately fit due to a flatter dipolar evolution.

We have used the potential of this method to analyze the influence of the KcsA C-terminal domain on the extent of lower gate motion. We confirmed that in the absence of antibody and crystal lattice contact, the CTD restricts lower gate movement, a finding in excellent agreement with the increased rate and extent of C-type inactivation accompanied by CTD truncation.⁴⁷ We also found that in the absence of any crystallographic lattice contact or Fab fragment attached to the protein, KcsA's lower gate opens approximately 6–8 Å, with a very wide

dynamic range, largely recapitulating the various degrees of opening observed by crystallography. Finally, the broadening of the distance distribution when KcsA opens has revealed the dynamic nature of the lower gate suggesting that upon activation, the lower gate populates multiple conformationally open states.

AUTHOR INFORMATION

Corresponding Author

eperozo@uchicago.edu

Author Contributions

[†]These authors contributed equally.

Notes

The authors declare no competing financial interest.

ACKNOWLEDGMENTS

The authors thank Dr. Gunnar Jeschke for feedback and helpful advice with DEER Analysis. We also thank Dr. Luis G. Cuello and members of the Perozo lab for technical advice and manuscript review. O.D. thanks the organizers of the EPR Workshop 2010: Cutting-Edge Biomedical EPR Methods, for a stimulating experience on the pulsed EPR technique. H.C.H. thanks Dr. Francisco Bezanilla for support by NIH Grant GM030376. This work was supported by NIH Grant GM088406.

REFERENCES

- (1) Perozo, E.; Cortes, D. M.; Somporpisut, P.; Kloda, A.; Martinac, B. *Nature* **2002**, *418*, 942.
- (2) Perozo, E.; Cuello, L. G.; Cortes, D. M.; Liu, Y. S.; Somporpisut, P. *Novartis Found. Symp.* **2002**, *245*, 146.
- (3) Claxton, D. P.; Quick, M.; Shi, L.; de Carvalho, F. D.; Weinstein, H.; Javitch, J. A.; Mchaourab, H. S. *Nat. Struct. Mol. Biol.* **2010**, *17*, 822.
- (4) Smirnova, I.; Kasho, V.; Choe, J. Y.; Altenbach, C.; Hubbell, W. L.; Kaback, H. R. *Proc. Natl. Acad. Sci. U.S.A.* **2007**, *104*, 16504.
- (5) Borbat, P. P.; Surendhran, K.; Bortolus, M.; Zou, P.; Freed, J. H.; Mchaourab, H. S. *PLoS Biol.* **2007**, *5*, No. e271.
- (6) Jeschke, G.; Polyhach, Y. *Phys. Chem. Chem. Phys.* **2007**, *9*, 1895.
- (7) Endeward, B.; Butterwick, J. A.; MacKinnon, R.; Prisner, T. F. *J. Am. Chem. Soc.* **2009**, *131*, 15246.
- (8) Jeschke, G.; Sajid, M.; Schulte, M.; Godt, A. *Phys. Chem. Chem. Phys.* **2009**, *11*, 6580.
- (9) Payandeh, J.; Scheuer, T.; Zheng, N.; Catterall, W. A. *Nature* **2011**, *475*, 353.
- (10) Catterall, W. A. *Cold Spring Harbor Perspect. Biol.* **2011**, *3*, No. a003947.
- (11) Doyle, D. A.; Morais Cabral, J.; Pfuetzner, R. A.; Kuo, A.; Gulbis, J. M.; Cohen, S. L.; Chait, B. T.; MacKinnon, R. *Science* **1998**, *280*, 69.
- (12) Lunin, V. V.; Dobrovetsky, E.; Khutoreskaya, G.; Zhang, R.; Joachimiak, A.; Doyle, D. A.; Bochkarev, A.; Maguire, M. E.; Edwards, A. M.; Koth, C. M. *Nature* **2006**, *440*, 833.
- (13) Chang, G.; Spencer, R. H.; Lee, A. T.; Barclay, M. T.; Rees, D. C. *Science* **1998**, *282*, 2220.
- (14) Hilf, R. J.; Dutzler, R. *Nature* **2008**, *452*, 375.
- (15) *Advanced ESR Methods in Polymer Research* Jeschke, G., Schlick, S., Eds.; Wiley-Interscience: Hoboken, NJ, 2006.
- (16) Jeschke, G.; Chechik, V.; Ionita, P.; Godt, A.; Zimmermann, H.; Banham, J.; Timmel, C. R.; Hilger, D.; Jung, H. *Appl. Magn. Reson.* **2006**, *30*, 473.
- (17) Tikhonov, A. N.; Arsenin, V. I. A. *Solutions of Ill-Posed Problems*; Winston: Washington, DC, 1977.
- (18) Hansen, P. C.; O'Leary, D. P. *SIAM J. Sci. Comput.* **1993**, *14*, 1487.
- (19) Domingo Kohler, S.; Spitzbarth, M.; Diederichs, K.; Exner, T. E.; Drescher, M. *J. Magn. Reson.* **2011**, *208*, 167.

- (20) Perozo, E.; Cortes, D. M.; Cuello, L. G. *Science* **1999**, *285*, 73.
- (21) Blunck, R.; Cordero-Morales, J. F.; Cuello, L. G.; Perozo, E.; Bezanilla, F. J. *Gen. Physiol.* **2006**, *128*, 569.
- (22) Baker, K. A.; Tzitzilonis, C.; Kwiatkowski, W.; Choe, S.; Riek, R. *Nat. Struct. Mol. Biol.* **2007**, *14*, 1089.
- (23) Ader, C.; Schneider, R.; Hornig, S.; Velisetty, P.; Wilson, E. M.; Lange, A.; Giller, K.; Ohmert, I.; Martin-Eauclaire, M. F.; Trauner, D.; Becker, S.; Pongs, O.; Baldus, M. *Nat. Struct. Mol. Biol.* **2008**, *15*, 605.
- (24) Cuello, L. G.; Jogini, V.; Cortes, D. M.; Perozo, E. *Nature* **2010**, *466*, 203.
- (25) Uysal, S.; Cuello, L. G.; Cortes, D. M.; Koide, S.; Kossiakoff, A. A.; Perozo, E. *Proc. Natl. Acad. Sci. U.S.A.* **2011**, *108*, 11896.
- (26) Dalmas, O.; Cuello, L. G.; Jogini, V.; Cortes, D. M.; Roux, B.; Perozo, E. *Structure* **2010**, *18*, 868.
- (27) Perozo, E.; Cortes, D. M.; Cuello, L. G. *Nat. Struct. Biol.* **1998**, *5*, 459.
- (28) Miller, K. S. *Multidimensional Gaussian Distributions*; Wiley: New York, 1964.
- (29) Jakeman, E.; Tough, R. J. A. *J. Opt. Soc. Am. A* **1987**, *4*, 1764.
- (30) Kohler, D. S.; Spitzbarth, M.; Diederichs, K.; Exner, T. E.; Drescher, M. J. *Magn. Reson.* **2011**, *208*, 167.
- (31) Eshaghi, S.; Niegowski, D.; Kohl, A.; Martinez Molina, D.; Lesley, S. A.; Nordlund, P. *Science* **2006**, *313*, 354.
- (32) Polyhach, Y.; Bordignon, E.; Jeschke, G. *Phys. Chem. Chem. Phys.* **2011**, *13*, 2356.
- (33) Fleissner, M. R.; Bridges, M. D.; Brooks, E. K.; Cascio, D.; Kálai, T.; Hideg, K.; Hubbell, W. L. *Proc. Natl. Acad. Sci. U.S.A.* **2011**, *108*, 16241.
- (34) Jeschke, G.; Koch, A.; Jonas, U.; Godt, A. *J. Magn. Reson.* **2002**, *155*, 72.
- (35) Jeschke, G.; Bender, A.; Paulsen, H.; Zimmermann, H.; Godt, A. *J. Magn. Reson.* **2004**, *169*, 1.
- (36) Beale, E. M. L. *J. R. Stat. Soc. B* **1960**, *22*, 41.
- (37) Seber, G. A. F.; Wild, C. J. *Nonlinear Regression*; Wiley: New York, 1989.
- (38) Straume, M.; Frasier-Cadore, S.; Johnson, M. In *Topics in Fluorescence Spectroscopy*; Lakowicz, J., Ed.; Plenum Press, New York: 1991; p 177.
- (39) Zhou, Y.; Morais-Cabral, J. H.; Kaufman, A.; MacKinnon, R. *Nature* **2001**, *414*, 43.
- (40) Morais-Cabral, J. H.; Zhou, Y.; MacKinnon, R. *Nature* **2001**, *414*, 37.
- (41) Yuan, P.; Leonetti, M. D.; Hsiung, Y.; MacKinnon, R. *Nature* **2012**, *481*, 94.
- (42) Wu, Y.; Yang, Y.; Ye, S.; Jiang, Y. *Nature* **2010**, *466*, 393.
- (43) Iscla, I.; Wray, R.; Blount, P. *Protein Sci.* **2011**, *20*, 1638.
- (44) Pau, V.; Zhu, Y.; Yuchi, Z.; Hoang, Q.; Yang, D. *J. Biol. Chem.* **2007**, *282*, 29163.
- (45) Cortes, D. M.; Cuello, L. G.; Perozo, E. *J. Gen. Physiol.* **2001**, *117*, 165.
- (46) Uysal, S.; Vasquez, V.; Tereshko, V.; Esaki, K.; Fellouse, F. A.; Sidhu, S. S.; Koide, S.; Perozo, E.; Kossiakoff, A. *Proc. Natl. Acad. Sci. U.S.A.* **2009**, *106*, 6644.
- (47) Cuello, L. G.; Jogini, V.; Cortes, D. M.; Pan, A. C.; Gagnon, D. G.; Dalmas, O.; Cordero-Morales, J. F.; Chakrapani, S.; Roux, B.; Perozo, E. *Nature* **2010**, *466*, 272.
- (48) Ader, C.; Schneider, R.; Hornig, S.; Velisetty, P.; Vardanyan, V.; Giller, K.; Ohmert, I.; Becker, S.; Pongs, O.; Baldus, M. *EMBO J.* **2009**, *28*, 2825.